Composite Structures 118 (2014) 217–227

Contents lists available at ScienceDirect

Composite Structures

journal homepage: www.elsevier.com/locate/compstruct

The role of shear deformation in laminated plates with curvilinear fiber paths and embedded defects

A.H. Akbarzadeh, M. Arian Nik, D. Pasini *

Department of Mechanical Engineering, McGill University, Macdonald Engineering Building, 817 Sherbrooke West, Montreal, QC H3A 0C3, Canada

ARTICLE INFO

Article history:
Available online 30 July 2014

Keywords:
Automated Fiber Placement
Fourier–Galerkin method
Gaps and overlaps
Moderately-thick laminated composite
Variable stiffness laminates

ABSTRACT

Automated Fiber Placement (AFP) is an advanced technology used to manufacture laminated composites with curvilinear fiber paths. During the manufacturing, AFP generally leads to the formation of defects, e.g. gaps and overlaps, that impact the laminate properties, to an extent that largely depends on the geometry, such as thickness and curvature, of the part. This paper focuses on moderately-thick laminate plates that present gaps and overlaps induced by AFP. We use higher-order shear deformation theories to study the role of shear deformation on the plate responses. A hybrid Fourier–Galerkin method is used to obtain a semi-analytic solution describing the static deformation of the plate. Eigenvalue analysis is also conducted to determine its fundamental frequency and critical buckling load. The numeric results show that shear deformation has a more severe impact on the structural responses of a variable stiffness than a constant stiffness plate. We find also that gaps deteriorate the structural performance, while overlaps improve it. Maps representing structural responses, in particular buckling vs. deflection and frequency vs. deflection, are generated to gain insight into the design of a variable stiffness laminate plate with defects.

1. Introduction

Laminated composite structures have drawn special attention from a variety of sectors including aerospace, automotive, naval, and construction. Composite laminates are generally built by stacking layers of dissimilar fiber orientation [1,2]. To achieve high strength-to-weight ratio, high stiffness-to-weight ratio, fatigue strength, and resistance to corrosion, composite laminates are designed with either constant or variable stiffness. In a constant-stiffness design, a laminate has layers of straight fibers that have the highest stiffness and strength when loaded along the fiber direction, whereas these properties are very low in the transverse direction. In a variable stiffness laminate, the fiber direction can be tailored to follow curvilinear fiber paths that best improve structural performance, such as buckling load [3–6], natural frequencies [7–9], and flexural stiffness [10]. Variable stiffness plates have also been demonstrated capable to offer trade-off properties that can concurrently optimize opposing requirements, such as buckling load and in-plane stiffness [4,11–13].

Several approaches exist in literature for the analysis of a laminated composite. Among them, equivalent single-layer (ESL) [14–16], three-dimensional (3D) elasticity [17–19], and multiple model methods [2] have been successfully used, each with a certain level of complexity. In this paper, we use ESL theory to reduce the computational effort required for the analysis of a variable-stiffness composite. With ESL, an equivalent two-dimensional (2D) layer is assumed to replace a heterogeneous 3D structure. The simplest ESL theory is the classical laminated plate theory (CLPT), whereby the lines that before deformation are straight and normal to the midplane of the laminate are assumed to keep these characteristics even after deformation. An outcome of this hypothesis is the neglect of the deformation caused by transverse shear (σ_{xz},σ_{yz}) and transverse normal (σ_{zz}) stresses. For moderately-thick composite laminates, such an assumption does not capture the real deformation of the composite laminate, thereby justifying the proposition of alternative shear deformation theories. For example, first-order shear deformation theory (FSDT) and third-order shear deformation theory (TSDT) have been introduced to account for deformation caused by transverse shear stresses [1,2,20–23]. FSDT assumes a constant shear strain through the thickness of a laminate and introduces a shear correction coefficient to compute transverse shear forces. TSDT, on the other hand,

* Corresponding author. Tel.: +1 514 398 6295; fax: +1 514 398 7365.
E-mail addresses: hamid.akbarzadeh@mcgill.ca (A.H. Akbarzadeh), mahdi.ariannik@mail.mcgill.ca (M. Arian Nik), damiano.pasini@mcgill.ca (D. Pasini).

http://dx.doi.org/10.1016/j.compstruct.2014.07.027
0263-8223/

uses a quadratic function to describe transverse shear stresses through the thickness, with vanishing values at the top and bottom surfaces of the laminate. As opposed to FSDT, TSDT avoids the need to introduce a shear correction factor [2].

FSDT and TSDT have been extensively used to model the structural mechanics of constant stiffness laminates as well as functionally graded (FG) beams and plates [24–27]. ESL and 3D elasticity theories were successfully applied to examine the buckling and postbuckling responses of laminated composites [17,28–33]. Other studies focused on the transient responses and resonance frequencies of free and forced vibration of laminated composites with constant stiffness [34–38]. FSDT and TSDT have been also used to study the static, as well as free and forced vibration, responses of heterogeneous plates and doubly curved panels [39–42]. Recently, a microstructure-dependent theory has been proposed for the static and dynamic analysis of FG beams and plates [43–45].

While there is a considerable amount of research that examines transverse shear deformation in constant stiffness composites, only a few studies look at variable stiffness laminates. One of these is that of Groh et al. [46], who studied via FSDT the impact of transverse shear deformation onto the flexural behavior of composite laminates with curvilinear fibers. It was shown that for a laminate with a length-to-thickness ratio of 10:1, an error of 43% may appear in the predicted transverse deflection if transverse shear stresses are neglected. Akhavan et al. [7,10] used the finite element method and TSDT to study the natural frequency and large deflection of a variable stiffness laminate. It was found that a variable stiffness design can remarkably reduce the deflection of a plate compared to a constant stiffness design and might yield improvement in the natural frequency.

Only until recently, the impact of defects within variable stiffness laminates was overlooked in literature. In practice, however, the formation of defects, mainly gaps and/or overlaps, is inevitable during the manufacturing of a variable stiffness laminate by Automated Fiber Placement (AFP). A method, namely "Defect layer", has been introduced [11,13] to appraise the effect of gaps and overlaps on the critical buckling load and in-plane stiffness of a thin laminate. It has been shown that gaps and overlaps can significantly change the buckling load and in-plane stiffness. In a study by Li et al. [47], it is suggested that gap areas can be filled with fibers from the layers above the gap, and those fibers dip down into gap areas. While this may be true in some cases, in this paper we assume that gap areas are relatively small; as such, the fibers bridge over the gaps rather than the dipping down. The outcome is that (1) gap regions are less stiff than those filled with composite fibers, (2) overlaps tend to generate stiffener-like features, which carry higher loads. With the recent use of AFP to build thick composite laminates for manned submersible applications [48], and moderately-thick composite laminates in megawatt-scale wind turbine blades [49], we turn our attention in this paper to thick and moderately-thick laminates with variable stiffness, with the goal of assessing the effect of gaps and overlaps on their structural performance. In particular, we use CLPT, FSDT, and TSDT theories to examine the global impact of transverse shear deformation on the structural responses of a variable stiffness plate with embedded defects. To account for the local effects induced by shear deformation, the reader is referred to [50–53] paper is organized as follows. In Section 2, we introduce geometric parameters that are used to model a curvilinear fiber path. Section 3 reviews the governing equations for structural analysis of variable stiffness plates using ESL theories. Next, a semi-analytic methodology using the hybrid Fourier–Galerkin method is developed to solve the governing differential equations. Finally, a discussion on the impact of shear stresses as well as defects induced by AFP on the structural behavior is presented before the closing remarks.

2. Variable stiffness laminate

A laminated plate manufactured with curvilinear fiber paths can be modeled by defining a reference fiber path along which the AFP machine places the first course. The subsequent fiber paths can be obtained by shifting the reference fiber path perpendicular to the steering direction. As a reference fiber path, we consider here one with constant curvature [54]. For this, the fiber orientation can be written as:

$$\cos\theta = \cos T_0 + \frac{|x|}{R}$$
$$R = \left|\frac{a/2}{[\cos(T_1) - \cos(T_0)]}\right| \tag{1}$$

where θ is the fiber orientation along the fiber path, T_0 and T_1 are respectively the fiber orientation at the plate midpoint and edges, R is the turning radius along the path, and a represents the plate width. The fiber orientation varies between T_0 (at the plate midpoint, $x = 0$) and T_1 (at the plate edges, $x = \pm\frac{a}{2}$), where the radius of the path remains constant (Fig. 1(a)). Since the fiber orientation changes along the x-direction, the reference fiber path should be shifted along the y-direction. A variable stiffness design is represented by $[\langle T_0|T_1\rangle]$, where $T_0 = T_1$ represents the case of straight fiber.

During the AFP process, the course width can be changed only by a discrete value, via either adding or dropping tows. As a result, defects in the form of gaps and overlaps emerge within the laminate. There are several strategies to add or drop a tow, such as complete gap and complete overlap strategies. With the former, a tow is cut as soon as one edge of the tow reaches a course boundary creating small triangular areas without fibers, i.e., gaps (Fig. 1(b)). With the latter, a tow is cut when both edges of the tow cross a course boundary, creating thickness buildup, i.e., overlaps (Fig. 1(c)) [55].

To obtain the effective stiffness matrices of a variable stiffness laminate with embedded defects, we use here the defect layer method, recently introduced in [11,13]. According to this method, a defect layer is similar to a regular composite layer with modified material properties, or thickness proportional to the defect area percentage. Compared to a regular composite layer, a gap-modified defect layer has the same thickness and reduced elastic properties, whereas an overlap-modified defect layer is thicker than a regular composite layer and has its elastic properties. For more details about the definition of a defect-layer, interested readers may refer to [13].

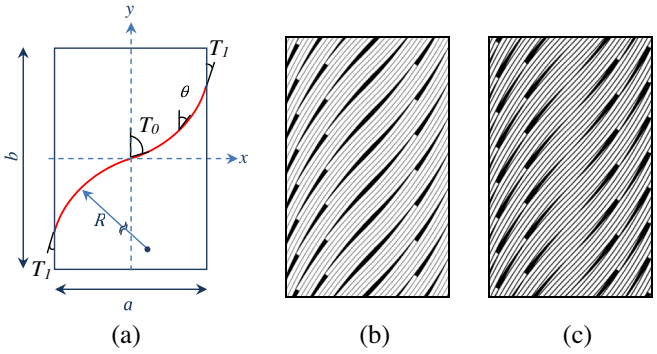

Fig. 1. (a) Fiber path definition; (b) gap (shaded area) distribution within the laminate; (c) overlap (shaded area) distribution within the laminate.

3. Problem definition and governing equations

Fig. 2 shows a rectangular laminated composite plate with length a, width b, and thickness h. We use here the CLPT to write displacement field as [2]:

$$\begin{aligned} u(x,y,z,t) &= u_0(x,y,t) - z\frac{\partial w_0(x,y,t)}{\partial x} \\ v(x,y,z,t) &= v_0(x,y,t) - z\frac{\partial w_0(x,y,t)}{\partial y} \\ w(x,y,z,t) &= w_0(x,y,t) \end{aligned} \tag{2}$$

where (u,v,w) are the displacement components along (x,y,z) coordinate axes and (u_0,v_0,w_0) stands for the displacement components of the midplane ($z = 0$).

Using the TSDT, the displacement field for a laminated plate can be written as [2,22]:

$$\begin{aligned} u(x,y,z,t) &= u_0(x,y,t) + z\phi_x(x,y,t) - c_1 z^3\left(\phi_x(x,y,t) + \frac{\partial w_0(x,y,t)}{\partial x}\right) \\ v(x,y,z,t) &= v_0(x,y,t) + z\phi_y(x,y,t) - c_1 z^3\left(\phi_y(x,y,t) + \frac{\partial w_0(x,y,t)}{\partial y}\right) \\ w(x,y,z,t) &= w_0(x,y,t) \end{aligned} \tag{3}$$

where ϕ_x and ϕ_y represent rotations about the x and y axes, respectively, and $c_1 = \frac{4}{3h^2}$. It is worth mentioning that Eq. (3) reduces to the FSDT displacement field formulation by setting $c_1 = 0$. For small strains and moderate rotations, the von-Karman strains in terms of the FSDT/TSDT displacement field given in Eq. (3) are written as follows [22]:

$$\begin{aligned} \begin{Bmatrix} \varepsilon_{xx} \\ \varepsilon_{yy} \\ \gamma_{xy} \end{Bmatrix} &= \begin{Bmatrix} \varepsilon^{(0)}_{xx} \\ \varepsilon^{(0)}_{yy} \\ \gamma^{(0)}_{xy} \end{Bmatrix} + z\begin{Bmatrix} \varepsilon^{(1)}_{xx} \\ \varepsilon^{(1)}_{yy} \\ \gamma^{(1)}_{xy} \end{Bmatrix} + z^3\begin{Bmatrix} \varepsilon^{(3)}_{xx} \\ \varepsilon^{(3)}_{yy} \\ \gamma^{(3)}_{xy} \end{Bmatrix}, \\ \begin{Bmatrix} \gamma_{yz} \\ \gamma_{xz} \end{Bmatrix} &= \begin{Bmatrix} \gamma^{(0)}_{yz} \\ \gamma^{(0)}_{xz} \end{Bmatrix} + z^2\begin{Bmatrix} \gamma^{(2)}_{yz} \\ \gamma^{(2)}_{xz} \end{Bmatrix} \end{aligned} \tag{4}$$

where

$$\begin{aligned} \begin{Bmatrix} \varepsilon^{(0)}_{xx} \\ \varepsilon^{(0)}_{yy} \\ \gamma^{(0)}_{xy} \end{Bmatrix} &= \begin{Bmatrix} u_{0,x} + \frac{1}{2}w^2_{0,x} \\ v_{0,y} + \frac{1}{2}w^2_{0,y} \\ u_{0,y} + v_{0,x} + w_{0,x}w_{0,y} \end{Bmatrix}, \quad \begin{Bmatrix} \varepsilon^{(1)}_{xx} \\ \varepsilon^{(1)}_{yy} \\ \gamma^{(1)}_{xy} \end{Bmatrix} = \begin{Bmatrix} \phi_{x,x} \\ \phi_{y,y} \\ \phi_{x,y} + \phi_{y,x} \end{Bmatrix}, \\ \begin{Bmatrix} \varepsilon^{(3)}_{xx} \\ \varepsilon^{(3)}_{yy} \\ \gamma^{(3)}_{xy} \end{Bmatrix} &= -c_1\begin{Bmatrix} \phi_{x,x} + w_{0,xx} \\ \phi_{y,y} + w_{0,yy} \\ \phi_{x,y} + \phi_{y,x} + 2w_{0,xy} \end{Bmatrix} \\ \begin{Bmatrix} \gamma^{(0)}_{yz} \\ \gamma^{(0)}_{xz} \end{Bmatrix} &= \begin{Bmatrix} \phi_y + w_{0,y} \\ \phi_x + w_{0,x} \end{Bmatrix}, \quad \begin{Bmatrix} \gamma^{(2)}_{yz} \\ \gamma^{(2)}_{xz} \end{Bmatrix} = -c_2\begin{Bmatrix} \phi_y + w_{0,y} \\ \phi_x + w_{0,x} \end{Bmatrix} \end{aligned} \tag{5}$$

and where the comma represents the partial differentiation operator, and $c_2 = 3c_1$. The strain–displacement equations given in Eqs. (4) and (5) have been written for TSDT; however, these equations could also be used for FSDT by setting $c_1 = c_2 = 0$. Moreover, substituting $\phi_x = -w_{0,x}$ and $\phi_y = -w_{0,y}$ into Eqs. (4) and (5) eliminates transverse shear strains and leads to the CLPT formulation.

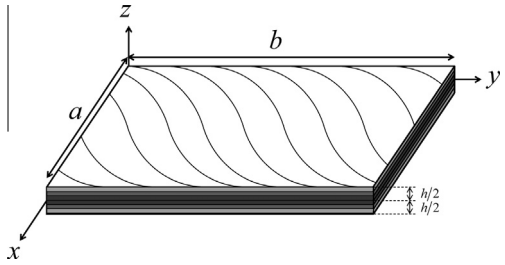

Fig. 2. Geometry of a rectangular laminated plate with a curvilinear fiber path.

The equations of motion for ESL theories, including classical and shear deformation theories, are derived by using the principle of virtual displacement; one can refer to [2] for further details. The equations of motion using the CLPT are written as [2,23]:

$$\begin{aligned} &N_{xx,x} + N_{xy,y} = I_0\ddot{u}_o - I_1\ddot{w}_{0,x} \\ &N_{xy,x} + N_{yy,y} = I_0\ddot{v}_o - I_1\ddot{w}_{0,y} \\ &M_{xx,xx} + 2M_{xy,xy} + M_{yy,yy} + \hat{N}(w_0) + q(x,y) \\ &\quad = I_0\ddot{w}_o - I_2(\ddot{w}_{0,xx} + \ddot{w}_{0,yy}) + I_1(\ddot{u}_{0,x} + \ddot{v}_{0,y}) \end{aligned} \tag{6}$$

while the FSDT/TSDT equations of motion are expressed as [20,22]:

$$\begin{aligned} &N_{xx,x} + N_{xy,y} = I_0\ddot{u}_o + J_1\ddot{\phi}_x - c_1 I_3\ddot{w}_{0,x} \\ &N_{xy,x} + N_{yy,y} = I_0\ddot{v}_o + J_1\ddot{\phi}_y - c_1 I_3\ddot{w}_{0,y} \\ &\overline{Q}_{x,x} + \overline{Q}_{y,y} + c_1(P_{xx,xx} + 2P_{xy,xy} + P_{yy,yy}) + \hat{N}(w_0) + q(x,y) \\ &\quad = I_0\ddot{w}_o - c_1^2 I_6(\ddot{w}_{0,xx} + \ddot{w}_{0,yy}) + c_1(I_3(\ddot{u}_{0,x} + \ddot{v}_{0,y}) + J_4(\ddot{\phi}_{x,x} + \ddot{\phi}_{y,y})) \\ &\overline{M}_{xx,x} + \overline{M}_{xy,y} - \overline{Q}_x = J_1\ddot{u}_o + K_2\ddot{\phi}_x - c_1 J_4\ddot{w}_{0,x} \\ &\overline{M}_{xy,x} + \overline{M}_{yy,y} - \overline{Q}_y = J_1\ddot{v}_o + K_2\ddot{\phi}_y - c_1 J_4\ddot{w}_{0,y} \end{aligned} \tag{7}$$

where

$$\begin{aligned} &(N_{\alpha\beta}, M_{\alpha\beta}, P_{\alpha\beta}) = \int_{-\frac{h}{2}}^{\frac{h}{2}} \sigma_{\alpha\beta}(1, z, z^3)dz, \quad (Q_\alpha, R_\alpha) = c_f\int_{-\frac{h}{2}}^{\frac{h}{2}} \sigma_{\alpha z}(1, z^2)dz \\ &\overline{M}_{\alpha\beta} = M_{\alpha\beta} - c_1 P_{\alpha\beta}, \quad \overline{Q}_\alpha = Q_\alpha - c_2 R_\alpha \\ &I_i = \int_{-\frac{h}{2}}^{\frac{h}{2}} \rho z^i dz, \quad J_i = I_i - c_1 I_{i+2}, \quad K_2 = I_2 - 2c_1 I_4 + c_1^2 I_6 \\ &\quad (i = 0, 1, \ldots, 6) \\ &\begin{cases} c_2 \neq 0, c_f = 1 & TSDT \\ c_2 = 0 & FSDT \end{cases} \end{aligned} \tag{8}$$

where $q(x,y)$ is the distributed transverse load at the bottom/top surface of the plate and α and β take the symbols x and y, $\sigma_{\alpha\beta}$ is the second Piola–Kirchhoff stress components, c_f is the shear correction factor, ρ is the mass density, and the superposed dot on a variable denotes the time derivation. It is worth noting that the determination of the shear correction factor (c_f) for FSDT is cumbersome since it depends on lamination properties, stacking sequence, geometric parameters, loading, and boundary conditions. Therefore in this work, we consider three values commonly used in literature, $c_f = 1$, $c_f = 5/6$, and $c_f = 3/4$ or homogeneous isotropic structures a correction factor of $c_f = \pi^2/12$, which is very close to $c_f = 5/6$, has been suggested in the literature [56–58]. To conduct a bifurcation buckling analysis, the nonlinear in-plane force resultant $\hat{N}(w_0)$ is written as [2,22]:

$$\hat{N}(w_0) = (N_{xx}w_{0,x} + N_{xy}w_{0,y})_{,x} + (N_{xy}w_{0,x} + N_{yy}w_{0,y})_{,y} \tag{9}$$

The stress resultants N, M, P, Q, and R are related to strains as [2,22]:

$$\begin{Bmatrix} \{N\} \\ \{M\} \\ \{P\} \end{Bmatrix} = \begin{bmatrix} [A] & [B] & [E] \\ [B] & [D] & [F] \\ [E] & [F] & [H] \end{bmatrix}\begin{Bmatrix} \{\varepsilon^{(0)}\} \\ \{\varepsilon^{(1)}\} \\ \{\varepsilon^{(3)}\} \end{Bmatrix} \tag{10a}$$

$$\begin{Bmatrix} \{Q\} \\ \{R\} \end{Bmatrix} = \begin{bmatrix} [A] & [D] \\ [D] & [F] \end{bmatrix}\begin{Bmatrix} \{\gamma^{(0)}\} \\ \{\gamma^{(2)}\} \end{Bmatrix} \tag{10b}$$

where the stiffness matrices are defined as:

$$(A_{ij}, B_{ij}, D_{ij}, E_{ij}, F_{ij}, H_{ij}) = \int_{-\frac{h}{2}}^{\frac{h}{2}} \overline{Q}_{ij}(1, z, z^2, z^3, z^4, z^6)dz \tag{11}$$

where $\overline{Q}_{ij}$ is the transformed plane stress-reduced stiffness.

The governing equations of CLPT and TSDT, which are not given for the sake of brevity, are derived by substituting Eqs. (4), (5), and (10) into Eqs. (6) and (7), respectively. Herein, the nonlinear terms for static and free vibration analyses are omitted; only the nonlinear in-plane force resultant $\hat{N}(w_0)$ is retained for buckling analysis. The governing partial differential equations are written for a specially orthotropic ($D_{16} = D_{26} = F_{16} = F_{26} = H_{16} = H_{26} = 0$) laminated composite with a balanced ($A_{16} = A_{26} = 0$) symmetric ($B_{ij} = E_{ij} = 0$) layup. We note that in contrast to constant stiffness composites, the elements of the stiffness matrices are a function of the spatial coordinates (x, y). In other words, the derivatives of these matrices with respect to x and y coordinates are not zero. As a result, the governing equations of motion for CLPT, FSDT, and TSDT are dissimilar from the conventional governing equations given for a constant stiffness composite.

4. Methodology

In this paper, we consider the following simply-supported boundary conditions:

$$\begin{aligned}
&v_0(0,y,t)=0, \quad v_0(a,y,t)=0, \quad u_0(x,0,t)=0, \quad u_0(x,b,t)=0\\
&\phi_y(0,y,t)=0, \quad \phi_y(a,y,t)=0, \quad \phi_x(x,0,t)=0, \quad \phi_x(x,b,t)=0\\
&w_0(0,y,t)=0, \quad w_0(a,y,t)=0, \quad w_0(x,0,t)=0, \quad w_0(x,b,t)=0\\
&N_{xx}(0,y,t)=0, \quad N_{xx}(a,y,t)=0, \quad N_{yy}(x,0,t)=0, \quad N_{yy}(x,b,t)=0\\
&\overline{M}_{xx}(0,y,t)=0, \quad \overline{M}_{xx}(a,y,t)=0, \quad \overline{M}_{yy}(x,0,t)=0, \quad \overline{M}_{yy}(x,b,t)=0
\end{aligned} \tag{12}$$

For CLPT analysis, the rotation terms ϕ_x and ϕ_y are neglected in the boundary conditions. Because of the presence of the derivatives of the stiffness matrices in the governing differential equations, the Galerkin method along with the Fourier series expansion are used to reach a semi-analytic solution. For the displacement fields in FSDT/TSDT analysis, we consider the Fourier series expansions that satisfy the boundary conditions in Eq. (12) [22,39]:

$$\begin{Bmatrix} u_0(x,y,t)\\ v_0(x,y,t)\\ w_0(x,y,t)\\ \phi_x(x,y,t)\\ \phi_y(x,y,t) \end{Bmatrix} = \sum_{n=1}^{n_y}\sum_{m=1}^{m_x} \begin{Bmatrix} U_{mn}(t)\cos(r_m x)\sin(r_n y)\\ V_{mn}(t)\sin(r_m x)\cos(r_n y)\\ W_{mn}(t)\sin(r_m x)\sin(r_n y)\\ X_{mn}(t)\cos(r_m x)\sin(r_n y)\\ Y_{mn}(t)\sin(r_m x)\cos(r_n y) \end{Bmatrix} \tag{13}$$

where $r_m = \frac{m\pi}{a}$, $r_n = \frac{n\pi}{b}$, U_{mn}, V_{mn}, W_{mn}, X_{mn}, and Y_{mn} are unknown coefficients that should be determined to satisfy the governing equations, with m and n as arbitrary integers for summation. Using the Galerkin method and the approximate displacement field (Eq. (13)), we can solve the governing differential equations for the FSDT/TSDT analysis [2,40]:

$$\int_{y=0}^{b}\int_{x=0}^{a} \begin{Bmatrix} R_1(U_{mn},V_{mn},W_{mn},X_{mn},Y_{mn})\cos(r_p x)\sin(r_q y)\\ R_2(U_{mn},V_{mn},W_{mn},X_{mn},Y_{mn})\sin(r_p x)\cos(r_q y\\ R_3(U_{mn},V_{mn},W_{mn},X_{mn},Y_{mn})\sin(r_p x)\cos(r_q y\\ R_4(U_{mn},V_{mn},W_{mn},X_{mn},Y_{mn})\sin(r_p x)\cos(r_q y\\ R_5(U_{mn},V_{mn},W_{mn},X_{mn},Y_{mn})\sin(r_p x)\cos(r_q y \end{Bmatrix} dxdy = 0 \tag{14}$$
$$(p = 1,2,\ldots,m_x,\ q = 1,2,\ldots,n_y)$$

where $R_i (i = 1,\ldots,5)$ are the residuals of the governing differential equations for the admissible displacement field (Eq. (13)). Substituting Eq. (13) into TSDT/FSDT governing equations and then applying Galerkin formulation (Eq. (14)), for laminates with symmetric layups ($B_{ij} = E_{ij} = 0$) and prescribed transverse shear modulus ($G_{xz} = G_{yz}$) in each lamina, leads to an expanded formulation (see Appendix A), which results in a $(5 \times m_x \times n_y) \times (5 \times m_x \times n_y)$ system of differential equations, here expressed as:

$$[K_{TSDT}]\{\Delta_{TSDT}\} + [M_{TSDT}]\{\ddot{\Delta}_{TSDT}\} = \{F_{TSDT}\} \tag{15}$$

where $\{\Delta_{TSDT}\}^T = \{U_{11}\ V_{11}\ W_{11}\ X_{11}\ Y_{11}\ \cdots\ U_{m_x n_y}\ V_{m_x n_y}\ W_{m_x n_y}\ X_{m_x n_y} Y_{m_x n_y}\}$, K_{TSDT} and M_{TSDT} are stiffness and mass matrices, and F_{TSDT} represents the mechanical force vector. If no $\hat{N}(w_0)$ exists, then there is no nonlinear in-plane force resultant, and the system of differential Eq. (15) can be solved for the static and free vibration analyses. For the transient analysis, the Newmark integration procedure can be adopted [2,22]. If $\hat{N}(w_0)$ is present, however, a bifurcation analysis is necessary to obtain the critical buckling load [2].

For CLPT analysis, the equations in Appendix A result in a $(3 \times m_x \times n_y) \times (3 \times m_x \times n_y)$ system of differential equations:

$$[K_{CLPT}]\{\Delta_{CLPT}\} + [M_{CLPT}]\{\ddot{\Delta}_{CLPT}\} = \{F_{CLPT}\} \tag{16}$$

where $\{\Delta_{CLPT}\}^T = \{U_{11}\ V_{11}\ W_{11}\ \cdots\ U_{m_x n_y}\ V_{n_x n_y}\ W_{m_x n_y}\}$. The equations above are numerically solved via MATLAB scripts developed for variable stiffness composite laminates with embedded defects.

5. Results and discussion

To validate the methodology presented in Section 4, we first compare the results available in literature for static bending, buckling, and natural vibration of plates with constant stiffness laminated composites. Then, we examine variable stiffness plates. In particular, we focus on the impact of shear stresses and manufacturing defects on their maximum static deflection, critical buckling load, and fundamental frequency.

5.1. Validation

As a case study, we consider a simply-supported plate with constant stiffness, symmetric cross-ply $[0/90]_s$ and planar square ($a = b = 1$ m) geometry. Its material properties are $E_1 = 175$ GPa, $E_2 = 7$ GPa, $G_{12} = G_{13} = 3.5$ GPa, $G_{23} = 1.4$ GPa, and $\nu_{12} = 0.25$. Table 1 shows the results of the dimensionless midpoint deflection $\left(\bar{w} = w_0\left(\frac{a}{2},\frac{b}{2}\right)\frac{E_2 h^3}{a^4 q_0}\right)$ of the plate subjected to a distributed transverse load ($q = q_0 \sin(r_m x)\sin(r_n y)$), obtained with FSDT, TSDT, and 3D elasticity. The results shows that all the predictions are very close to those provided in [2]. For a plate with the length-to-thickness ratio of $a/h = 4$, the FSDT and TSDT show a discrepancy of 12.5% and 3%, respectively, compared to the solution obtained with 3D elasticity.

Table 2 shows the dimensionless uniaxial critical buckling load $\left(\overline{N} = \frac{N_{cr}a^2}{E_2 h^3}\right)$ and fundamental frequency $\left(\bar{\omega} = \frac{\omega a^2}{h}\sqrt{\frac{\rho}{E_2}}\right)$ as a function of the modulus ratio E_1/E_2 for $a/h = 5$ and 10, where $G_{12} = G_{13} = 0.6E_2$, $G_{23} = 0.5E_2$, and $\nu_{12} = 0.25$. Similar to the case of maximum deflection, the application of FSDT/TSDT leads to an accuracy improvement, compared to CLPT, in calculating the critical buckling load and natural frequency. The results given in Tables 1 and 2 indicate that the difference between the results predicted by FSDT and TSDT is much more evident in the maximum deflection than in the critical buckling load and natural frequency.

5.2. Structural responses of variable stiffness laminates

In this section, we use CLPT, FSDT, and TSDT to study the influence of manufacturing defects on the structural responses of

Table 1
Dimensionless maximum deflection of a simply-supported, symmetric, and cross-ply $[0/90]_s$ plate under a sinusoidally distributed transverse load.

	a/h	TSDT	TSDT [2]	FSDT*	FSDT* [2]	3D Elasticity [59]
$\bar{w} \times 10^2$	4	1.8937	1.894	1.7091	1.71	1.954
	10	0.7146	0.715	0.6625	0.6625	0.743

* The correction factor is $c_f = 5/6$.

Table 2
Dimensionless critical uniaxial buckling load and fundamental frequency of a simply-supported, symmetric, and cross-ply $[0/90]_s$ plate.

	a/h	E_1/E_2	TSDT	TSDT [2]	FSDT*	FSDT* [2]	3D Elasticity [60,61]
$\bar{N}$	10	20	15.2984	15.298	15.3513	15.351	15.019
		40	23.34	23.34	23.4529	23.453	22.881
$\bar{\omega}$	5	20	9.5625	9.526	9.566	9.567	9.56
		40	10.821	10.787	10.8529	10.854	10.752

* The correction factor is $c_f = 5/6$.

variable stiffness plates. We consider a square plate ($a = b = 1$ m) made of 16-ply balanced and symmetric laminate with a variable stiffness design of $[\pm\langle 58|39\rangle]_{4s}$. The material properties of prepreg composites and resin that are used for the analysis of constant and variable stiffness laminates are given in Table 3. It is worth mentioning that the effective material properties of variable stiffness laminates, obtained with the defect layer method, spatially change throughout the laminate as a function of the fiber orientation (Eq. (1), which depends on the turning radius along the path, the plate width, and the embedded defects. The structural responses of the plate, including static deflection, uniaxial critical buckling load, and fundamental frequency, are compared with those of a quasi-isotropic (QI) plate, here selected as a baseline. The QI plate considered in this study has the following layup: $[45/0/-45/90]_{2s}$. The plate is subjected to a uniform transverse loading, $q(x,y,t) = q_0(t)$, for static analysis.

5.2.1. Static analysis

The maximum out-of-plane deflection occurs at the plate mid-point, as shown in Table 4 for a set of length-to-thickness ratios (a/h). For a very thin plate ($a/h = 200$), all ESL theories predict very close maximum deflection. However for the length-to-thickness ratio $a/h = 20$, discrepancies up to 7% emerge from CLPT and TSDT results. For a very thick laminate with $a/h = 5$, differences are greater than 55%. Furthermore, the discrepancy between ESL theories depends on the embedded manufacturing defects. For instance, for a plate with $a/h = 10$, incorporating the effect of overlap increases the deviation by about 3% compared to the defect-free case, whereas considering the effect of gap decreases the discrepancy by 2%. These trends can be attributed to the emergence of overlaps, which are thickness build-ups that decrease the overall length-to-thickness ratio of the plate in comparison with the defect-free case. On the other hand, a variable stiffness plate with gaps has effective elastic properties lower than a defect-free plate with higher length-to-thickness ratio.

Fig. 3 shows the out-of-plane mid-span deflection ($y = b/2$) for a plate with $a/h = 10$ for the cases: defect-free, complete gap, and complete overlap. The trends reveal the importance of accounting for the manufacturing defects in the analysis of variable stiffness laminates. Compared to the defect-free case, the out-of-plane deflection of a plate changed with respect to the type of defects considered. For instance, for a plate with gaps, the maximum out-of-plane deflection increases by 9% compared to the defect-free case, whereas a decrease of 24% is observed for a plate with overlaps. The reason for this difference is attributed to the morphology of a defect. Gaps are resin-rich areas that lower the plate out-of-plane stiffness, whereas overlaps along the fiber paths are thickness build-ups that increase it.

5.2.2. Buckling analysis

Table 5 reports the critical buckling load obtained with alternative ESL theories, and manufacturing strategies. The values are

Table 3
Material properties of prepreg composite and resin.

	E_1 (GPa)	E_2 (GPa)	G_{12} (GPa)	G_{13} (GPa)	G_{23} (GPa)	ν_{12}	ρ (kg/m^3)
Prepreg	143	9.1	4.82	4.9	4.9	0.3	1500
Resin	3.72	3.72	1.43	1.43	1.43	0.3	1100

Table 4
Dimensionless maximum deflection ($\bar{w} \times 100$) under uniform static load.

a/h	Layup	Manufacturing defects	CLPT	FSDT			TSDT
				$c_f = 1$	$c_f = 5/6$	$c_f = 3/4$	
5	QI	–	0.6970	1.2974	1.4174	1.4973	1.3968
	$[\pm\langle 58|39\rangle]_{4s}$	Defect-free	0.5787	1.1784	1.2989	1.3793	1.2902
		Complete gap	0.6483	1.2474	1.3679	1.4482	1.3601
		Complete overlap	0.4233	0.9651	1.0738	1.1464	1.0139
10	QI	–	0.6970	0.8473	0.8773	0.8973	0.8735
	$[\pm\langle 58|39\rangle]_{4s}$	Defect-free	0.5787	0.7269	0.7569	0.7769	0.7567
		Complete gap	0.6483	0.7963	0.8263	0.8463	0.8262
		Complete overlap	0.4233	0.5578	0.5848	0.6029	0.5739
20	QI	–	0.6970	0.7346	0.7421	0.7471	0.7413
	$[\pm\langle 58|39\rangle]_{4s}$	Defect-free	0.5787	0.6145	0.6219	0.6269	0.6223
		Complete gap	0.6483	0.6841	0.6915	0.6965	0.6918
		Complete overlap	0.4233	0.4565	0.4632	0.4677	0.4606
200	QI	–	0.6970	0.6974	0.6975	0.6975	0.6975
	$[\pm\langle 58|39\rangle]_{4s}$	Defect-free	0.5787	0.5775	0.5775	0.5776	0.5779
		Complete gap	0.6483	0.6471	0.6472	0.6472	0.6475
		Complete overlap	0.4233	0.4232	0.4232	0.4233	0.4230

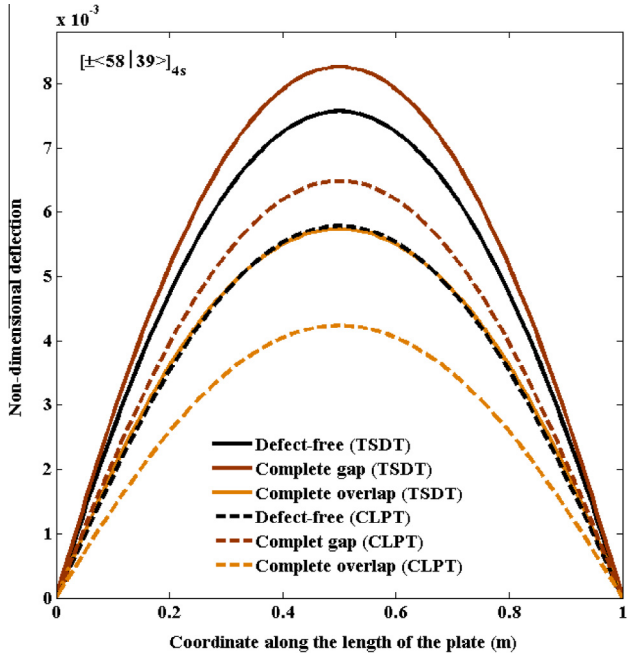

Fig. 3. Non-dimensional deflection of the variable stiffness plate at the middle width of the plate.

given for several length-to-thickness ratios of a plate loaded in the x-direction. Table 5 shows significant discrepancies between the results predicted with CLPT and TSDT. In particular for a plate with $a/h = 20$ and $a/h = 5$, the discrepancies between results obtained with CLPT and TSDT increase from 7% to 177% respectively. Comparing Tables 4 and 5 reveals that shear stresses have an impact on the buckling load severer than that on the maximum out-of-plane deflection. For example, for a plate with $a/h = 10$, the difference between the CLPT and TSDT results for the maximum deflection is 23%, while this value is greater than 33% for buckling. We can also observe that – compared to a defect-free case – gaps embedded in a variable stiffness plate reduce the buckling load, whereas overlaps increase it. For $a/h = 10$, the buckling load reduces by 8% for a plate with gaps, whereas it increases by 31% for a plate with overlaps. Among the considered shear correction factors in FSDT analysis, the results in Table 5 show that $c_f = 5/6$ leads to the most accurate results compared to the TSDT's.

5.2.3. Free vibration analysis

Table 6 shows the impact of length-to-thickness ratio, manufacturing defects, and ESL theories on the fundamental frequency of a variable stiffness plate. From a comparison of CLPT and TSDT results (Table 6), a discrepancy greater than 4% can be observed for a plate with $a/h = 20$; this value increases up to 48% for a thick plate with $a/h = 5$. Comparing Tables 4–6 reveals that the differences between CLPT and TSDT is the least for fundamental frequency, followed by maximum out-of-plane deflection and critical buckling load. As shown in Table 6, variable stiffness plates with gaps have a fundamental frequency lower than defect-free laminates, whereas plates with overlaps have a higher value. The presence of gaps in a variable stiffness plate with $a/h = 10$, for example, reduces the natural frequency by 3%, while overlaps increase it by 10% when compared to a defect-free case.

5.3. Influence of curvilinear fiber path

As explained in Section 2 for a variable stiffness laminate with a constant curvature fiber path, the geometric parameters T_0 and T_1 define the fiber path trajectory. This section examines the impact of T_0 and T_1 on the structural responses of a variable stiffness plate. For the plate here under investigation, Fig. 4 illustrates the gap and overlap area percentages as a function of T_0 and T_1 over the entire design space. The white areas represent plate designs that do not satisfy the manufacturing constraint, i.e., the minimum turning radius of 0.635 m imposed by a typical AFP machine. For straight-fiber laminates ($T_0 = T_1$), no gaps or overlaps appear in the laminate, whereas the area percentage for both gaps and overlaps increases when the difference between T_0 and T_1 becomes larger.

We examine a plate with $a/h = 10$ for different manufacturing strategies. Fig. 5 illustrates its critical buckling load and fundamental frequency versus maximum deflection, each normalized by the corresponding values of a quasi-isotropic laminate. As opposed to a constant stiffness design, whose response domain is represented by a line, a variable stiffness design yields to domains of larger extent. Furthermore, in comparison with the results obtained for a defect-free plate, overlaps shift the response domain towards a higher buckling load and lower maximum deflection. On the other hand, gaps shift the domain towards a lower buckling load and higher deflection. This behavior is attributed to the effect of overlaps, which are thickness build-ups that tend to stiffen the plate along the fiber path, thereby improving its structural responses. In contrast gaps, resin-rich areas with reduced mechanical

Table 5
Non-dimensional critical uniaxial buckling load $\overline{N}$.

a/h	Layup	Manufacturing defects	CLPT	FSDT			TSD
				$c_f = 1$	$c_f = 5/6$	$c_f = 3/4$	
5	QI	–	22.9449	11.0145	9.6400	8.8997	10.0207
	$[\pm\langle 58\vert 39\rangle]_{4s}$	Defect-free	27.3871	11.0053	9.6240	8.8359	9.8807
		Complete gap	24.4371	10.6500	9.3505	8.6476	9.5668
		Complete overlap	37.4079	12.8441	11.0096	10.0458	12.6159
10	QI	–	22.9449	18.5992	17.9207	17.4953	17.9966
	$[\pm\langle 58\vert 39\rangle]_{4s}$	Defect-free	27.3871	21.4298	20.5281	19.9680	20.5376
		Complete gap	24.4371	19.5815	18.8261	18.3541	18.8325
		Complete overlap	37.4079	27.8196	26.4589	25.6235	26.9924
20	QI	–	22.9449	21.6782	21.4415	21.2866	21.4654
	$[\pm\langle 58\vert 39\rangle]_{4s}$	Defect-free	27.3871	25.6575	25.3244	25.1071	25.3122
		Complete gap	24.4371	23.0510	22.7818	22.6059	22.7720
		Complete overlap	37.4079	34.4681	33.9274	33.5763	34.1331
200	QI	–	22.9449	22.9315	22.9289	22.9271	22.9291
	$[\pm\langle 58\vert 39\rangle]_{4s}$	Defect-free	27.3871	27.4449	27.4410	27.4384	27.4256
		Complete gap	24.4371	24.4829	24.4798	24.4778	24.4676
		Complete overlap	37.4079	37.4199	37.4134	37.4091	37.4386

Table 6
Dimensionless fundamental frequency $\bar{\omega}$.

a/h	Layup	Manufacturing defects	CLPT	FSDT			TSDT
				$c_f = 1$	$c_f = 5/6$	$c_f = 3/4$	
5	QI	–	14.5766	10.7240	10.2568	9.9767	10.3671
	$[\pm\langle 58\vert 39\rangle]_{4s}$	Defect-free	15.9252	11.2059	10.6708	10.3534	10.7471
		Complete gap	15.2834	11.0643	10.5641	10.2655	10.6347
		Complete overlap	17.7628	11.8632	11.2461	10.8838	11.6402
10	QI	–	14.9262	13.4755	13.2324	13.0775	13.2773
	$[\pm\langle 58\vert 39\rangle]_{4s}$	Defect-free	16.3072	14.4699	14.1679	13.9767	14.1887
		Complete gap	15.6500	14.0493	13.7810	13.6103	13.8008
		Complete overlap	18.2697	15.8181	15.4348	15.1940	15.6165
20	QI	–	15.0177	14.6004	14.5210	14.4689	14.5347
	$[\pm\langle 58\vert 39\rangle]_{4s}$	Defect-free	16.4071	15.8846	15.7819	15.7145	15.7841
		Complete gap	15.7459	15.2962	15.2073	15.1489	15.2098
		Complete overlap	18.4033	17.6699	17.5320	17.4418	17.5953
200	QI	–	15.0482	15.0438	15.0429	15.0423	15.0431
	$[\pm\langle 58\vert 39\rangle]_{4s}$	Defect-free	16.4404	16.4578	16.4566	16.4559	16.4521
		Complete gap	15.7779	15.7926	15.7916	15.7910	15.7878
		Complete overlap	18.4481	18.4510	18.4494	18.4483	18.4558

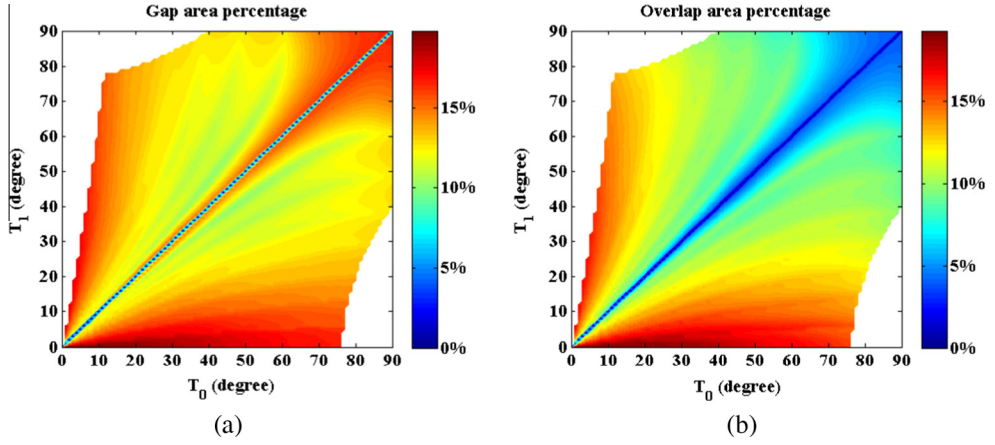

Fig. 4. (a) Complete gap area percentage and (b) complete overlap area percentage as a function of T_0 and T_1 for a variable stiffness plate.

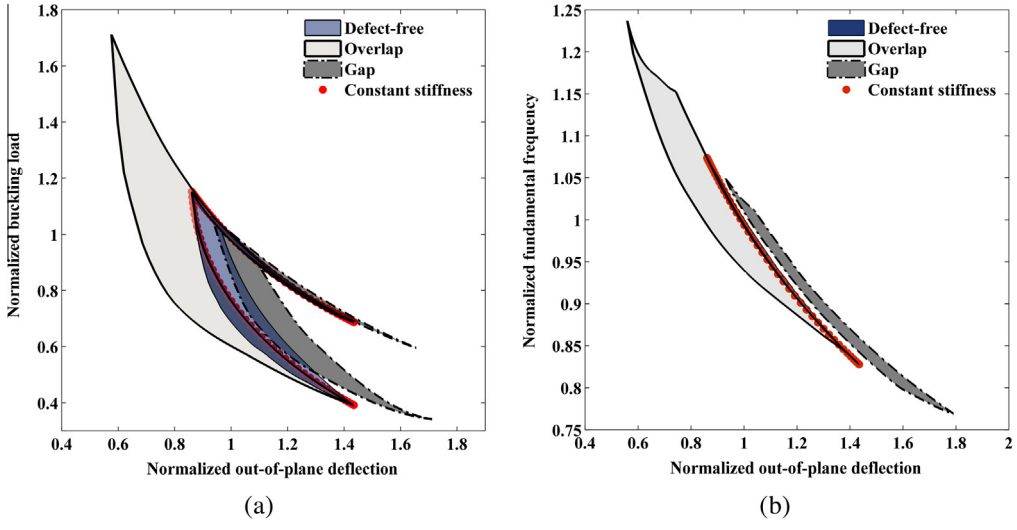

Fig. 5. Plate response domains for (a) buckling-deflection and (b) fundamental frequency-deflection in different manufacturing scenarios.

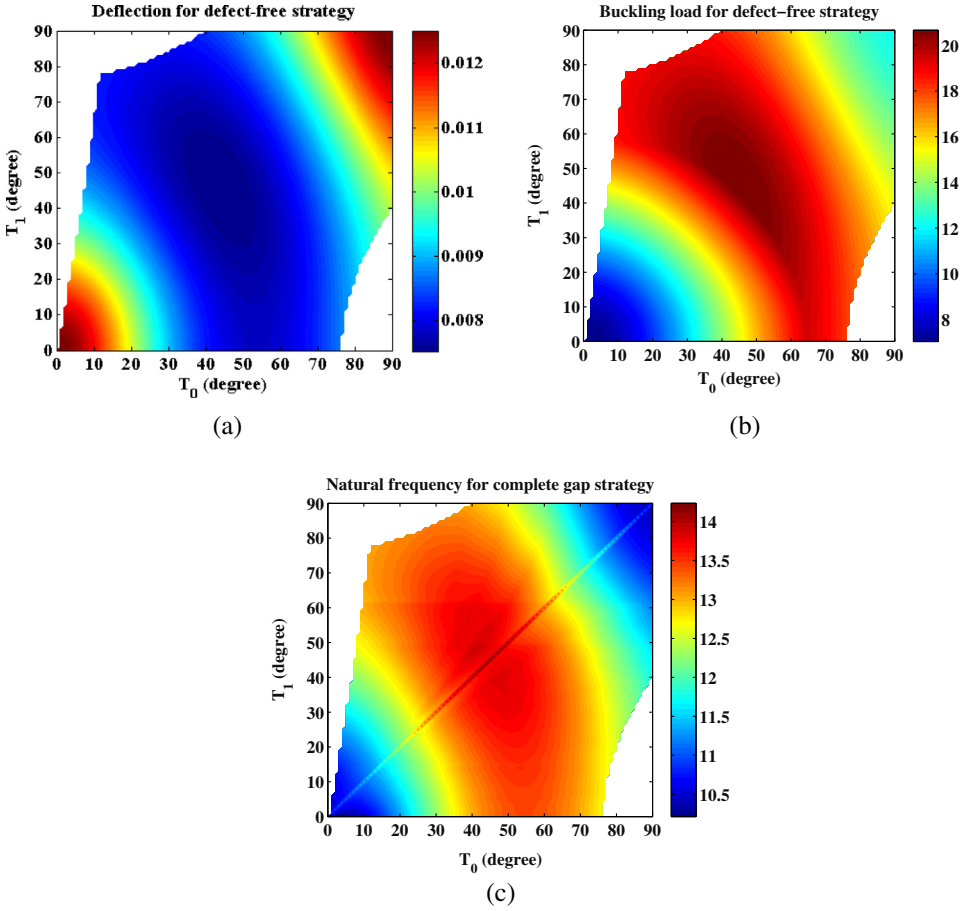

Fig. 6. (a) Non-dimensional maximum deflection($\bar{w}$), (b) critical buckling load ($\overline{N}$), and (c) natural frequency ($\bar{\omega}$) of a defect-free variable stiffness plate.

properties, deteriorate the structural responses of the plate. As shown in Fig. 4(a), a complete gap strategy yields a large amount of gaps. In contrast, a complete overlap strategy results in an amount of overlap that continuously increases as the fiber path deviates from the straight path. As a result, a remarkable difference exists between the boundary of the feasible domain of a plate with gaps and the one with straight fibers. A similar behavior can be observed in the domain fundamental frequency versus maximum deflection. From a comparison of Fig. 5(a) and (b), we observe that the buckling-deflection domain for a defect-free plate is significantly larger than the corresponding frequency-deflection domain. Since, the effectiveness of a variable stiffness laminate depends on the boundary conditions [4], we gather that for a variable stiffness plate other loading and boundary conditions can result in a larger response domain.

To isolate the effect of the curvilinear fiber path from the effect of gaps and overlaps, we plot in Fig. 6 the fiber path curvature versus the maximum deflection, critical buckling load, and fundamental frequency. As can be seen, the regions offering low deflection correspond to regions with high critical buckling and fundamental frequency. Bearing in mind that fibers located along the loading direction result in the highest in-plane stiffness but not in the lowest deflection, we see here the opportunity to find trade-offs between in-plane and out-of-plane performance under vibration and buckling constraints. This study requires further work.

6. Conclusions

This paper has examined the effect of transverse shear deformation and embedded manufacturing defects on the structural responses of a variable stiffness plate made by AFP. Static bending, buckling, and free vibration have been studied. We have first presented the governing equations obtained via classical and shear deformation theories, and then solved them by using the hybrid Fourier–Galerkin method. For very thin plates, all ESL theories provide close results. However, for moderately-thick plates with length-to-thickness ratio $a/h = 10$, major differences emerge between CLPT and TSDT predictions. In particular, discrepancies up to 23%, 33%, and 15% are observed for the maximum out-of-plane deflection, critical buckling load, and fundamental frequency.

The results obtained in this paper show the important role played by shear deformation in moderately-thick plates with variable stiffness, where the macroscopic mechanical properties spatially vary. We have also highlighted that the discrepancy between ESL theories depends on the amount of the embedded defects. In a static bending analysis of a plate with $a/h = 10$, incorporating the effects of overlaps increases the discrepancy of the maximum deflection calculated with CLPT and TSDT, up to 26%. On the other hand, considering the effect of gaps results in about 22% difference. Finally maps have been presented to show how the structural responses of a defected plate change with respect to a defect-free plate.

Appendix A

The hybrid Fourier–Galerkin form of the governing differential equations for FSDT/TSDT analysis of laminated plates, with symmetric layups ($B_{ij} = E_{ij} = 0$) and given transverse shear modulus in each lamina, can be written as follows:

$$\sum_{n=1}^{n_y}\sum_{m=1}^{m_x}\int_{y=0}^{b}\int_{x=0}^{a}\Big\{\big[(-A_{11}r_m^2-A_{66}r_n^2)\cos(r_mx)\sin(r_ny)$$
$$-A_{11,x}r_m\sin(r_mx)\sin(r_ny)+A_{66,y}r_n\cos(r_mx)\cos(r_ny)\big]U_{mn}(t)$$
$$+[-(A_{12}+A_{66})r_mr_n\cos(r_mx)\sin(r_ny)+A_{66,y}r_m\cos(r_mx)\cos(r_ny)$$
$$-A_{12,x}r_n\sin(r_mx)\sin(r_ny)]V_{mn}(t)-[I_0\cos(r_mx)\sin(r_ny)]\ddot{U}_{mn}(t)$$
$$-\big[J_1\cos(r_mx)\sin(r_ny)\big]\ddot{X}_{mn}-\big[-c_1I_3r_m\cos(r_mx)\sin(r_ny)\big]\ddot{W}_{mn}\Big\}$$
$$\times\cos(r_px)\sin(r_qy)dxdy=0 \qquad (A.1a)$$

$$\sum_{n=1}^{n_y}\sum_{m=1}^{m_x}\int_{y=0}^{b}\int_{x=0}^{a}\{[-(A_{12}+A_{66})r_mr_n\sin(r_mx)\cos(r_ny)$$
$$+A_{66,x}r_n\cos(r_mx)\cos(r_ny)-A_{12,y}r_m\sin(r_mx)\sin(r_ny)]U_{mn}(t)$$
$$+\big[(-A_{22}r_n^2-A_{66}r_m^2)\sin(r_mx)\cos(r_ny)-A_{22,y}r_n\sin(r_mx)\sin(r_ny)$$
$$+A_{66,x}r_m\cos(r_mx)\cos(r_ny)\big]V_{mn}(t)-[I_0\sin(r_mx)\cos(r_ny)]\ddot{V}_{mn}(t)$$
$$-[J_1\sin(r_mx)\cos(r_ny)]\ddot{Y}_{mn}-[-c_1I_3r_n\sin(r_mx)\cos(r_ny)]\ddot{W}_{mn}\}$$
$$\times\sin(r_px)\cos(r_qy)dxdy=0 \qquad (A.1b)$$

$$\sum_{n=1}^{n_y}\sum_{m=1}^{m_x}\int_{y=0}^{b}\int_{x=0}^{a}\{[(-(c_fA_{55}-2c_2D_{55}+c_2^2F_{55}-c_1^2(H_{11,xx}+H_{12,yy}))r_m^2$$
$$-(c_fA_{44}-2c_2D_{44}+c_2^2F_{44}-c_1^2(H_{12,xx}+H_{22,yy}))r_n^2$$
$$-c_1^2H_{11}r_m^4-2c_1^2(H_{12}+2H_{66})r_m^2r_n^2-c_1^2H_{22}r_n^4)\sin(r_mx)\sin(r_ny)$$
$$+((c_fA_{55,x}-2c_2D_{55,x}+c_2^2F_{55,x})r_m+2c_1^2H_{11,x}r_m^3$$
$$+(2c_1^2H_{12,x}+4c_1^2H_{66,x})r_mr_n^2)\cos(r_mx)\sin(r_ny)$$
$$+(2c_1^2H_{22,y}r_n^3+(c_fA_{44,y}-2c_2D_{44,y}+c_2^2F_{44,y})r_n$$
$$-(-2c_1^2H_{12,y}-4c_1^2H_{66,y})r_m^2r_n)\sin(r_mx)\cos(r_ny)$$
$$-4c_1^2H_{66,xy}r_mr_n\cos(r_mx)\cos(r_ny)]W_{mn}$$
$$+[((c_fA_{55,x}-2c_2D_{55,x}+c_2^2F_{55,x})-(2c_1F_{66,x}-2c_1^2H_{66,x})r_n^2$$
$$-(2c_1F_{11,x}-2c_1^2H_{11,x})r_m^2)\cos(r_mx)\sin(r_ny)$$
$$+(-(c_fA_{55}-2c_2D_{55}+c_2^2F_{55}+c_1F_{11,xx}$$
$$-c_1^2(H_{11,xx}+H_{12,yy})+c_1F_{12,yy})r_m+(c_1F_{11}-c_1^2H_{11})r_m^3$$
$$+(c_1F_{12}+2c_1F_{66}-c_1^2(2H_{66}+H_{12})r_mr_n^2)\sin(r_mx)\sin(r_ny)$$
$$-(2c_1F_{12,y}-2c_1^2H_{12,y}+2c_1F_{66,y}-2c_1^2H_{66,y})r_mr_n\sin(r_mx)\cos(r_ny)$$
$$+(2c_1F_{66,xy}-2c_1^2H_{66,xy})r_n\cos(r_mx)\cos(r_ny)]X_{mn}$$
$$+[((c_fA_{44,y}-2c_2D_{44,y}+c_2^2F_{44,y})-(2c_1F_{22,y}-2c_1^2H_{22,y})r_n^2$$
$$-(2c_1F_{66,y}-2c_1^2H_{66,y})r_m^2)\sin(r_mx)\cos(r_ny)$$
$$+(-(c_fA_{44}-2c_2D_{44}+c_2^2F_{44}+c_1F_{22,yy}-c_1^2(H_{12,xx}+H_{22,yy})$$
$$+c_1F_{12,xx})r_n+(c_1F_{22}-c_1^2H_{22})r_n^3$$
$$+(c_1F_{12}+2c_1F_{66}-c_1^2(2H_{66}+H_{12})r_m^2r_n)\sin(r_mx)\sin(r_ny)$$
$$-(2c_1F_{12,x}-2c_1^2H_{12,x}+2c_1F_{66,x}-2c_1^2H_{66,x})r_mr_n\cos(r_mx)\sin(r_ny)$$
$$+(2c_1F_{66,xy}-2c_1^2H_{66,xy})r_m\cos(r_mx)\cos(r_ny)]Y_{mn}$$
$$-[N_{xx}^0r_m^2+N_{yy}^0r_n^2]\sin(r_mx)\sin(r_ny)W_{mn}+q(x,y,t)$$
$$+[c_1I_3r_m]\sin(r_mx)\sin(r_ny)\ddot{U}_{mn}+[c_1I_3r_n]\sin(r_mx)\sin(r_ny)\ddot{V}_{mn}$$
$$-[I_0+c_1I_6(r_m^2+r_n^2)]\sin(r_mx)\sin(r_ny)\ddot{W}_{mn}$$
$$+[J_4r_m]\sin(r_mx)\sin(r_ny)\ddot{X}_{mn}$$
$$+[J_4r_n]\sin(r_mx)\sin(r_ny)\ddot{Y}_{mn}\}\sin(r_px)\sin(r_qy)dxdy=0 \qquad (A.1c)$$

$$\sum_{n=1}^{n_y}\sum_{m=1}^{m_x}\int_{y=0}^{b}\int_{x=0}^{a}\{[(-(-c_1F_{11}+c_1^2H_{11})r_m^3$$
$$-(-c_1F_{12}+c_1^2H_{12}-2c_1F_{66}+2c_1^2H_{66})r_mr_n^2$$
$$+(-c_fA_{55}+2c_2D_{55}-c_2^2F_{55})r_m)\cos(r_mx)\sin(r_ny)$$
$$+(-(-c_1F_{11,x}+c_1^2H_{11,x})r_m^2$$
$$-(-c_1F_{12,x}+c_1^2H_{12,x})r_n^2)\sin(r_mx)\sin(r_ny)$$
$$+(-2c_1F_{66,y}+2c_1^2H_{66,y})r_mr_n\cos(r_mx)\cos(r_ny)]\}W_{mn}(t)$$
$$+[(-(D_{11}-2c_1F_{11}+c_1^2H_{11})r_m^2-(D_{66}-2c_1F_{66}+c_1^2H_{66})r_n^2$$
$$+(-c_fA_{55}+2c_2D_{55}-c_2^2F_{55}))\cos(r_mx)\sin(r_ny)$$
$$-(D_{11,x}-2c_1F_{11,x}+c_1^2H_{11,x})r_m\sin(r_mx)\sin(r_ny)$$
$$+(D_{66,y}-2c_1F_{66,y}+c_1^2H_{66,y})r_n\cos(r_mx)\cos(r_ny)]X_{mn}$$
$$+[-(D_{12}-2c_1F_{12}-2c_1F_{66}+c_1^2H_{12}+c_1^2H_{66}+D_{66})r_mr_n$$
$$\times\cos(r_mx)\sin(r_ny)+(D_{66,y}-2c_sF_{66,y}+c_s^2H_{66,y})r_m$$
$$\times\cos(r_mx)\cos(r_ny)-(D_{12,x}-2c_1F_{12,x}+c_1^2H_{12,x})r_n$$
$$\times\sin(r_mx)\sin(r_ny)]Y_{mn}-[J_1\cos(r_mx)\sin(r_ny)]\ddot{U}_{mn}$$
$$-[-c_1J_4r_m\cos(r_mx)\sin(r_ny)]\ddot{W}_{mn}$$
$$-[K_2\cos(r_mx)\sin(r_ny)]\ddot{X}_{mn}\}\cos(r_px)\sin(r_qy)dxdy \qquad (A.1d)$$

$$\sum_{n=1}^{n_y}\sum_{m=1}^{m_x}\int_{y=0}^{b}\int_{x=0}^{a}\{[(-(-c_1F_{22}+c_1^2H_{22})r_n^3$$
$$-(-c_1F_{12}+c_1^2H_{12}-2c_1F_{66}+2c_1^2H_{66})r_m^2r_n$$
$$+(-c_fA_{44}+2c_2D_{44}-c_2^2F_{44})r_n)\sin(r_mx)\cos(r_ny)$$
$$+(-(-c_1F_{22,y}+c_1^2H_{22,y})r_n^2$$
$$-(-c_1F_{12,y}+c_1^2H_{12,y})r_m^2)\sin(r_mx)\sin(r_ny)$$
$$+(-2c_1F_{66,x}+2c_1^2H_{66,x})r_mr_n\cos(r_mx)\cos(r_ny)]\}W_{mn}(t)$$
$$+[-(D_{12}-2c_1F_{12}-2c_1F_{66}+c_1^2H_{12}+c_1^2H_{66}+D_{66})r_mr_n\sin(r_mx)$$
$$\times\cos(r_ny)+(D_{66,x}-2c_1F_{66,x}+c_1^2H_{66,x})r_n\cos(r_mx)\cos(r_ny)$$
$$-(D_{12,y}-2c_1F_{12,y}+c_1^2H_{12,y})r_m\sin(r_mx)\sin(r_ny)]X_{mn}$$
$$+[(-(D_{22}-2c_1F_{22}+c_1^2H_{22})r_n^2$$
$$-(D_{66}-2c_1F_{66}+c_1^2H_{66})r_m^2(-c_fA_{44}+2c_2D_{44}-c_2^2F_{44}))$$
$$\times\sin(r_mx)\cos(r_ny)-(D_{22,y}-2c_1F_{22,y}+c_1^2H_{22,y})r_n$$
$$\times\sin(r_mx)\sin(r_ny)+(D_{66,x}-2c_1F_{66,x}+c_1^2H_{66,x})r_m\cos(r_mx)\cos(r_ny)]Y_{mn}$$
$$-[J_1\sin(r_mx)\cos(r_ny)]\ddot{V}_{mn}-[-c_1J_4r_n\sin(r_mx)\cos(r_ny)]\ddot{W}_{mn}$$
$$-[K_2\sin(r_mx)\cos(r_ny)]\ddot{X}_{mn}\}\sin(r_px)\cos(r_qy)dxdy \qquad (A.1e)$$

The hybrid Fourier–Galerkin form of the governing differential equations for CLPT analysis is also written as:

$$\sum_{n=1}^{n_y}\sum_{m=1}^{m_x}\int_{y=0}^{b}\int_{x=0}^{a}\{[-A_{11,x}r_m\sin(r_mx)\sin(r_ny)$$
$$-(A_{11}r_m^2+A_{66}r_n^2)\cos(r_mx)\sin(r_ny)+A_{66,y}r_n\cos(r_mx)\cos(r_ny)]U_{mn}$$
$$+[-A_{12,x}r_n\sin(r_mx)\sin(r_ny)-(A_{12}+A_{66})r_mr_n\cos(r_mx)\sin(r_ny)$$
$$+A_{66,y}r_m\cos(r_mx)\cos(r_ny)]V_{mn}-I_0\cos(r_mx)\sin(r_ny)\ddot{U}_{mn}$$
$$+I_1r_m\cos(r_mx)\sin(r_ny)\ddot{W}_{mn}\}\cos(r_px)\sin(r_qy)dxdy=0 \qquad (A.2a)$$

$$\sum_{n=1}^{n_y}\sum_{m=1}^{m_x}\int_{y=0}^{b}\int_{x=0}^{a}\{[-A_{12,y}r_m\sin(r_mx)\sin(r_ny)$$
$$-(A_{12}+A_{66})r_mr_n\sin(r_mx)\cos(r_ny)+A_{66,x}r_n\cos(r_mx)\cos(r_ny)]U_{mn}$$
$$+[-A_{22,y}r_n\sin(r_mx)\sin(r_ny)-(A_{22}r_n^2+A_{66}r_m^2)\sin(r_mx)\cos(r_ny)$$
$$+A_{66,x}r_m\cos(r_mx)\cos(r_ny)]V_{mn}-I_0\sin(r_mx)\cos(r_ny)\ddot{V}_{mn}$$
$$+I_1r_n\sin(r_mx)\cos(r_ny)\ddot{W}_{mn}\}\sin(r_px)\cos(r_qy)dxdy=0 \qquad (A.2b)$$

$$\sum_{n=1}^{n_y}\sum_{m=1}^{m_x}\int_{y=0}^{b}\int_{x=0}^{a}\{[(D_{11,xx}r_m^2 - D_{11}r_m^4 + D_{12,xx}r_n^2 - 2D_{12}r_m^2r_n^2 + D_{12,yy}r_m^2 + D_{22,yy}r_n^2 - D_{22}r_n^4 - 4D_{66}r_m^2r_n^2)\sin(r_mx)\sin(r_ny) + (2D_{11,x}r_m^3 + 2D_{12,x}r_mr_n^2 + 4D_{66,x}r_mr_n^2)\cos(r_mx)\sin(r_ny) - 4D_{66,xy}r_mr_n\cos(r_mx)\cos(r_ny) + (2D_{22,y}r_n^3 + 2(D_{12,y} + 2D_{66,y})r_m^2r_n)\sin(r_mx)\cos(r_ny)]W_{mn} - [(N_{xx}^0r_m^2 + N_{yy}^0r_n^2)\sin(r_mx)\sin(r_ny)]W_{mn} + q(x,y,t) - I_1r_m\sin(r_mx)\sin(r_ny)\ddot{U}_{mn} - I_1r_n\sin(r_mx)\sin(r_ny)\ddot{V}_{mn} - [I_0 + I_2(r_m^2 + r_n^2)]\sin(r_mx)\sin(r_ny)\ddot{W}_{mn}\}\sin(r_px)\sin(r_qy)dxdy = 0 \quad (A.2c)$$

References

[1] Reddy JN, Arciniega R. Shear deformation plate and shell theories: from Stavsky to present. Mech Adv Mater Struct 2004;11:535–82.
[2] Reddy JN. Mechanics of laminated composite plates and shells: theory and analysis. CRC press; 2003.
[3] Alhajahmad A, Abdalla MM, Gürdal Z. Optimal design of tow-placed fuselage panels for maximum strength with buckling considerations. J Aircraft 2010;47:775–82.
[4] Arian Nik M, Fayazbakhsh K, Pasini D, Lessard L. Surrogate-based multi-objective optimization of a composite laminate with curvilinear fibers. Compos Struct 2012;94:2306–13.
[5] Gürdal Z, Tatting BF, Wu C. Variable stiffness composite panels: effects of stiffness variation on the in-plane and buckling response. Compos Part A: Appl Sci Manuf 2008;39:911–22.
[6] Setoodeh S, Abdalla MM, IJsselmuiden ST, Gürdal Z. Design of variable-stiffness composite panels for maximum buckling load. Compos Struct 2009;87:109–17.
[7] Akhavan H, Ribeiro P. Natural modes of vibration of variable stiffness composite laminates with curvilinear fibers. Compos Struct 2011;93:3040–7.
[8] Honda S, Narita Y. Vibration design of laminated fibrous composite plates with local anisotropy induced by short fibers and curvilinear fibers. Compos Struct 2011;93:902–10.
[9] Honda S, Narita Y. Natural frequencies and vibration modes of laminated composite plates reinforced with arbitrary curvilinear fiber shape paths. J Sound Vib 2012;331:180–91.
[10] Akhavan H, Ribeiro P, de Moura M. Large deflection and stresses in variable stiffness composite laminates with curvilinear fibres. Int J Mech Sci 2013;73:14–26.
[11] Arian Nik M, Fayazbakhsh K, Pasini D, Lessard L. Optimization of variable stiffness composites with embedded defects induced by automated fiber placement. Compos Struct 2014;107:160–6.
[12] Arian Nik M, Fayazbakhsh K, Pasini D, Lessard L. A comparative study of metamodeling methods for the design optimization of variable stiffness composites. Compos Struct 2014;107:494–501.
[13] Fayazbakhsh K, Arian Nik M, Pasini D, Lessard L. Defect layer method to capture effect of gaps and overlaps in variable stiffness laminates made by automated fiber placement. Compos Struct 2013;97:245–51.
[14] Komeili A, Akbarzadeh AH, Doroushi A, Eslami MR. Static analysis of functionally graded piezoelectric beams under thermo-electro-mechanical loads. Adv Mech Eng 2011:2011.
[15] Liu G, Zhao X, Dai K, Zhong Z, Li G, Han X. Static and free vibration analysis of laminated composite plates using the conforming radial point interpolation method. Compos Sci Technol 2008;68:354–66.
[16] Mantari J, Guedes Soares C. Generalized layerwise HSDT and finite element formulation for symmetric laminated and sandwich composite plates. Compos Struct 2013;105:319–31.
[17] Lee SY. Finite element dynamic stability analysis of laminated composite skew plates containing cutouts based on HSDT. Compos Sci Technol 2010;70:1249–57.
[18] Liu FL. Static analysis of thick rectangular laminated plates: three-dimensional elasticity solutions via differential quadrature element method. Int J Solids Struct 2000;37:7671–88.
[19] Zhong Z, Yu T. Analytical solution of a cantilever functionally graded beam. Compos Sci Technol 2007;67:481–8.
[20] Praveen G, Reddy J. Nonlinear transient thermoelastic analysis of functionally graded ceramic-metal plates. Int J Solids Struct 1998;35:4457–76.
[21] Reddy JN. An evaluation of equivalent-single-layer and layerwise theories of composite laminates. Compos Struct 1993;25:21–35.
[22] Reddy JN. Analysis of functionally graded plates. Int J Numer Methods Eng 2000;47:663–84.
[23] Reddy JN, Wang C. An overview of the relationships between solutions of the classical and shear deformation plate theories. Compos Sci Technol 2000;60:2327–35.
[24] Kant T, Swaminathan K. Analytical solutions for free vibration of laminated composite and sandwich plates based on a higher-order refined theory. Compos Struct 2001;53:73–85.
[25] Makhecha D, Ganapathi M, Patel B. Dynamic analysis of laminated composite plates subjected to thermal/mechanical loads using an accurate theory. Compos Struct 2001;51:221–36.
[26] Mantari J, Oktem A, Guedes Soares C. Static and dynamic analysis of laminated composite and sandwich plates and shells by using a new higher-order shear deformation theory. Compos Struct 2011;94:37–49.
[27] Sahoo R, Singh B. A new shear deformation theory for the static analysis of laminated composite and sandwich plates. Int J Mech Sci 2013;75:324–36.
[28] Han SC, Lee S-Y, Rus G. Postbuckling analysis of laminated composite plates subjected to the combination of in-plane shear, compression and lateral loading. Int J Solids Struct 2006;43:5713–35.
[29] Lee SY, Park D-Y. Buckling analysis of laminated composite plates containing delaminations using the enhanced assumed strain solid element. Int J Solids Struct 2007;44:8006–27.
[30] Spencer A, Watson P. Buckling of laminated anisotropic plates under cylindrical bending. J Mech Phys Solids 1992;40:1621–35.
[31] Tarn JQ. Elastic buckling of multilayered anisotropic plates. J Mech Phys Solids 1996;44:389–411.
[32] Wang S, Srinivasan S, Hu H, HajAli R. Effect of material nonlinearity on buckling and postbuckling of fiber composite laminated plates and cylindrical shells. Compos Struct 1995;33:7–15.
[33] Wang X. Differential quadrature for buckling analysis of laminated plates. Comput Struct 1995;57:715–9.
[34] Aydogdu M, Timarci T. Vibration analysis of cross-ply laminated square plates with general boundary conditions. Compos Sci Technol 2003;63:1061–70.
[35] Huang XL, Shen H-S, Zheng J-J. Nonlinear vibration and dynamic response of shear deformable laminated plates in hygrothermal environments. Compos Sci Technol 2004;64:1419–35.
[36] Lee WH, Han S-C. Free and forced vibration analysis of laminated composite plates and shells using a 9-node assumed strain shell element. Comput Mech 2006;39:41–58.
[37] Qing G, Qiu J, Liu Y. Free vibration analysis of stiffened laminated plates. Int J Solids Struct 2006;43:1357–71.
[38] Zhang W, Zhao M, Guo X. Nonlinear responses of a symmetric cross-ply composite laminated cantilever rectangular plate under in-plane and moment excitations. Compos Struct 2013;100:554–65.
[39] Akbarzadeh AH, Abbasi M, Hosseini zad SK, Eslami MR. Dynamic analysis of functionally graded plates using the hybrid Fourier–Laplace transform under thermomechanical loading. Meccanica 2011;46:1373–92.
[40] Akbarzadeh AH, Abbasi M, Eslami MR. Coupled thermoelasticity of functionally graded plates based on the third-order shear deformation theory. Thin-Walled Struct 2012;53:141–55.
[41] Akbarzadeh AH, Hosseini zad SK, Eslami MR, Sadighi M. Mechanical behaviour of functionally graded plates under static and dynamic loading. Proc Inst Mech Eng Part C: J Mech Eng Sci 2011;225:326–33.
[42] Kiani Y, Akbarzadeh AH, Chen ZT, Eslami MR. Static and dynamic analysis of an FGM doubly curved panel resting on the Pasternak-type elastic foundation. Compos Struct 2012;94:2474–84.
[43] Arbind A, Reddy J. Nonlinear analysis of functionally graded microstructure-dependent beams. Compos Struct 2013;98:272–81.
[44] Reddy JN. Microstructure-dependent couple stress theories of functionally graded beams. J Mech Phys Solids 2011;59:2382–99.
[45] Reddy J, Kim J. A nonlinear modified couple stress-based third-order theory of functionally graded plates. Compos Struct 2012;94:1128–43.
[46] Groh R, Weaver P, White S, Raju G, Wu Z. A 2D equivalent single-layer formulation for the effect of transverse shear on laminated plates with curvilinear fibres. Compos Struct 2013;100:464–78.
[47] Li X, Hallet SR, Wisnom MR. Modelling the effect of gaps and overlaps in automated fibre placement (AFP) manufactured laminates. In:19th international conference on composite materials; 2013.
[48] New manned submersible to feature carbon fiber composite hull. Composites World; 2013.
[49] Griffin DA, Ashwill TD. Alternative composite materials for megawatt-scale wind turbine blades: design considerations and recommended testing. In: ASME 2003 wind energy symposium: american society of mechanical engineers; 2003. p. 191–201.
[50] Fazzolari FA, Carrera E. Advanced variable kinematics Ritz and Galerkin formulations for accurate buckling and vibration analysis of anisotropic laminated composite plates. Compos Struct 2011;94:50–67.
[51] Tornabene F, Fantuzzi N, Viola E, Carrera E. Static analysis of doubly-curved anisotropic shells and panels using CUF approach, differential geometry and differential quadrature method. Compos Struct 2014;107:675–97.
[52] Tornabene F, Viola E, Fantuzzi N. General higher-order equivalent single layer theory for free vibrations of doubly-curved laminated composite shells and panels. Compos Struct 2013;104:94–117.
[53] Ferreira AJM, Carrera E, Cinefra M, Viola E, Tornabene F, Fantuzzi N, et al. Analysis of thick isotropic and cross-ply laminated plates by generalized differential quadrature method and a unified formulation. Compos Part B Eng 2014;58:544–52.
[54] Blom AW, Lopes CS, Kromwijk PJ, Gurdal Z, Camanho PP. A theoretical model to study the influence of tow-drop areas on the stiffness and strength of variable-stiffness laminates. J Compos Mater 2009;43:403–25.
[55] Tatting BF, Gurdal Z. Automated finite element analysis of elastically-tailored plates. NASA contractor report no NASA/CR-2003-212679; 2003.

[56] Altenbach H. On the determination of transverse shear stiffnesses of orthotropic plates. Z. Angew. Math. Phys. 2000;51:629–49.
[57] Bert CW. Simplified analysis of static shear factors for beams of nonhomogeneous cross section. J Compos Mater 1973;7:525–9.
[58] Altenbach H. An alternative determination of transverse shear stiffnesses for sandwich and laminated plates. Int J Solids Struct 2000;37:3503–20.
[59] Pagano N, Hatfield HJ. Elastic behavior of multilayered bidirectional composites. AIAA J 1972;10:931–3.
[60] Noor AK. Free vibrations of multilayered composite plates. AIAA J 1973;11:1038–9.
[61] Noor AK. Stability of multilayered composite plates. Fibre Sci Technol 1975;8:81–9.